Clays and Clay Minerals, Vol. 58, No. 1, 21–36, 2010.

STRESS-INDUCED ALTERATION OF SUDOITE: STRUCTURAL AND CHEMICAL MODIFICATIONS

María Dolores Ruiz Cruz[1,*], María Dolores Rodríguez Ruiz[1], and Carlos Sanz de Galdeano[2]

[1] Facultad de Ciencias, Campus de Teatinos, 29071 Málaga, Spain
[2] Instituto Andaluz de Ciencias de la Tierra, CSIC-Universidad de Granada, Facultad de Ciencias, 18071 Granada, Spain

Abstract—The purpose of this study was to investigate the structural and chemical modifications of phyllosilicates that occur under natural conditions, using the progressive deformation of chlorite (sudoite) present in quartz-rich veins from the Internal Zone of the Rif range (Morocco) as the model system. Signs of chlorite deformation include kinks, chevron-like folds, and fractures. The samples also contain later, undeformed grains, which sealed the fractures or grew with (001) perpendicular to the compressive stress. Deformation-induced structural changes consist mainly of basal cleavages associated with ordered replacement of brucite sheets by hydrated layers, thus leading to irregular microdomains of mixed-layer chlorite-vermiculite and sudoite. Such structural modifications represent a mechanism for accommodating the compressive stress. Structural changes were accompanied by minor chemical ones, which lead from di,tri-chlorite (sudoite) to phases with a more trioctahedral character (mixed-layer chlorite-vermiculite). The hydration reaction occurred throughout a topotactic replacement of the pre-existing sudoite grains. Later, undeformed grains consist of mixed-layer chlorite-vermiculite intergrown with retrogressive kaolinite and minor Fe oxide, and are interpreted as having formed through a dissolution-precipitation process, during deformation. Retrogression of sudoite probably occurred during the latest stage of exhumation, in low-temperature conditions.

Key Words—Chlorite-vermiculite, Clinochlore, Deformation, Mixed-layer, SEM, Sudoite, TEM-AEM.

INTRODUCTION

Quartz-, carbonate-, or plagioclase-bearing veins found in metamorphic terranes are generally interpreted to have formed during metamorphism through a process of metamorphic differentiation or segregation, as defined by Kretz (1994). Generally, the minerals found in a given vein are also constituents of the enclosing metamorphic rocks. The composition of the vein phases and of the enclosing rocks are, in most cases, similar (Kretz, 1994). Based on these observations, the general assumption is that the vein-forming elements in this case were derived from the immediately surrounding rocks.

Strongly deformed quartz veins are common in Permo-Triassic metapelites from the Internal Zone Complexes of the Betic-Rif range. In the northernmost part of the Beni Mezala window (Figure 1), some veins contain very small amounts of other metamorphic phases, including Ca-silicate (pumpellyite + actinolite + epidote) and kyanite + chloritoid assemblages. Carpholite-bearing veins have not been found at this zone but carpholite pseudomorphs have been described in other areas of the window. Veins generally contain minor amounts of trioctahedral chlorite but sudoite had only been described in veins from the tectonically overlying Boquete de Anyera unit. Veins are interpreted as having formed during prograde metamorphism, and preservation of some metamorphic phases has permitted the accurate determination of the metamorphic conditions affecting these formations, especially of those characterizing the high-pressure/low-temperature (H*P*-L*T*) alpine event (*e.g*. Goffé *et al*., 1989; Azañón *et al.*, 1992; Bouybaouène, 1993; Azañón and Goffé, 1997; Ruiz Cruz *et al.*, 2010).

Deformation affecting veins from the Betic-Rif range is generally observed at both the field and thin-section scales. Plastic deformation in metals and in some rock-forming minerals, such as quartz, carbonates, or feldspars, has been studied extensively (see Kretz, 1994, and references therein). Generally, plastic deformation occurs due to gliding, and is favored in most structures by the presence of dislocations. Plastic deformation generally leads in a first step to migration of the dislocations and formation of clusters of dislocations or polygonization. As the process advances, new dislocation-free crystals grow at the expense of the strained crystals. Stress-induced deformation in phyllosilicates is mainly due to basal slip, is favored by the presence of planar and linear defects, and leads to several types of folds and cleavages, with or without chemical perturbations (Baronnet and Olives, 1983; Bell and Wilson, 1981, 1986; Bell *et al*., 1986; Amouric, 1987).

Strongly deformed phyllosilicates (mainly micas and chlorite) are common in metamorphic terranes and numerous examples of the compositional changes

* E-mail address of corresponding author:
mdruiz@uma.es
DOI: 10.1346/CCMN.2010.0580102

associated with the dissolution-precipitation processes caused by deformation can be found, which can be used for interpreting the metamorphic history of the rocks. Nevertheless, although the mechanisms of deformation in phyllosilicates have been studied extensively under laboratory conditions and in natural samples (*e.g.* Vernon, 1977; Knipe, 1981; Bell and Wilson, 1981; Amouric, 1987) the structural and chemical modifications associated with natural deformations have been investigated to a lesser extent (*e.g.* Olives *et al.*, 1983; Sánchez-Navas and Galindo-Zaldívar, 1993; Ooteman *et al*., 2003; Jiménez-Millán *et al*., 2007), and devoted in most cases to biotite chloritization. An illustrative example of the structural and compositional modifications associated with progressive deformation of chlorite (sudoite) present in quartz-rich veins from the Internal Zone of the Rif range is presented here. The veins studied present a single mineral assemblage: quartz + 'chlorite,' which permitted interpretation of the XRD patterns and textures.

SAMPLES AND METHODOLOGY

Strongly deformed sudoite-bearing synfolial quartz veins, from Permo-Triassic, talc-bearing phyllites of the deepest Federico unit near Ceuta (Figure 1) were studied by X-ray diffraction (XRD) and scanning and transmission electron microscopy (SEM-TEM). These units have alternately been considered as typical Sebtide units (Kornprobst, 1971–1974; Bouybaouène, 1993) or as units intermediate between typical Ghomaride and Sebtide ones (Didon *et al.*, 1973; Sanz de Galdeano *et al*., 2001). Previous studies have indicated that materials from this unit record a H*P*/L*T* alpine event, as indicated by the presence of carpholite (Bouybaouène *et al*., 1995) although lower-grade pumpellyite-bearing assemblages have also been identified (Ruiz Cruz *et al*., 2010). The pressure peak was followed by a temperature increase during pressure release and subsequent exhumation.

'Chlorite'-enriched areas of the samples were obtained manually, and studied by petrographic microscopy, XRD, and scanning (SEM) and transmission-analytical (TEM/AEM) electron microscopy. The electron microprobe was not used because of the small size of the phyllosilicate grains. In addition, SEM permitted the observation of back-scattered images at larger scale and a more accurate selection of the analyzed areas. The XRD patterns of almost pure 'chlorite' separates were recorded using a Philips X'Pert PRO MPD (University of Málaga), with CuKα radiation and a Ge monochromator, operated at 40 mA and 40 kV with 0.01º2θ step size and 2 s counting time per step. Oriented samples, in the natural state, after ethylene-glycol solvation and after heating at 550ºC were used for phyllosilicate identification. Randomly oriented samples were used to determine the *b* parameter of phyllosilicates.

Polished and carbon-coated thin sections of areas of quartz veins containing 'chlorite' were imaged using back-scattered electrons and analyzed using a ZEISS DSM 950 scanning electron microscope (SEM), equipped with an X-ray energy dispersive (EDX) system (LINK QX 2000) at an accelerating voltage of 14 kV and 2 nA beam current (CIC, Granada University). The standards were albite (Na), orthoclase (K), periclase (Mg), wollastonite (Si and Ca), and synthetic oxides (Al_2O_3, Fe_2O_3, and $MnTiO_3$).

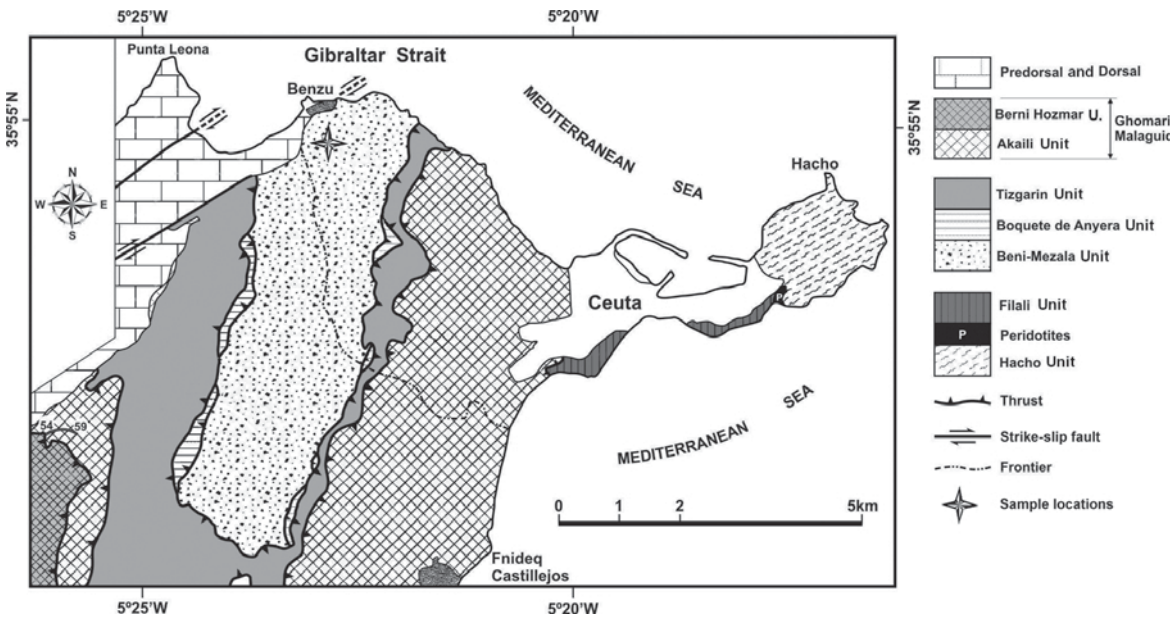

Figure 1. Tectonic map of the northern area of the Rif and location of the samples described in this paper (✦).

Several 'chlorite'-rich areas with different textural characteristics, as described below, were selected from thin sections and ion thinned for the TEM-AEM study. Transmission electron microscopy was performed at Granada University (CIC), with a 200 kV Philips CM-20 transmission electron microscope, fitted with a scanning transmission device (STEM) and solid-state detector for energy-dispersive analysis (EDX). Microanalyses were obtained in STEM mode. Quantitative determinations used the thin-film approximation of Cliff and Lorimer (1975). Albite (Na), muscovite and annite (K), albite, spessartine and muscovite (Al), forsterite and annite (Mg and Fe), spessartine (Mn), and titanite (Ca and Ti) were used as standards.

RESULTS

Petrography

The veins studied, up to 10 cm thick, are enclosed in talc-bearing white phyllites. The mineral assemblage of the enclosing rocks consists, in order of decreasing abundance, of white mica, talc, and minor chlorite, in addition to quartz, albite, K-feldspar, and rutile. Retrogressive phases, which appear to have grown during the compressive stage, are vermiculite and mixed-layer chlorite-vermiculite (Figure 2). In contrast, veins consist only of dominant quartz and a green phyllosilicate, not observed during the petrographic observation of the enclosing phyllites. The phyllosilicate appears enclosed in quartz and filling mm-sized veins cutting the larger quartz veins (Figure 3a). Quartz and phyllosilicate veins appear extensively deformed. Quartz crystals show undulatory extinction, and recrystallization of smaller quartz crystals is frequent (Figure 3a).

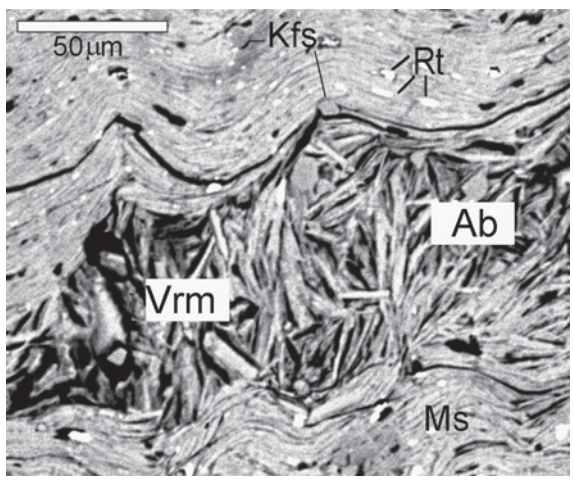

Figure 2. Back-scattered image showing textures characterizing the enclosing talc-bearing samples. Unoriented aggregates of dominant vermiculite (Vrm), and minor albite (Ab) appear to have grown during compressive stress. Kfs: K-feldspar; Ms: muscovite; Rt: rutile.

The green phyllosilicate, which strongly resembles chlorite, shows important variations in color, pleochroism, birefringence, and texture among several areas of the vein or even among adjacent grains. The intensity of color varied in parallel with the intensity of pleochroism and of the interference color and birefringence (<0.01 to >0.03). Levels of deformation are very variable; some grains are only slightly deformed (Figure 3b); others appear strongly deformed (Figure 3c,d); and minor grains, which have basal planes perpendicular to the compressive stress, are undeformed (Figure 3c,d). Such features, together with the associated chemical variations (see below), suggest the presence of at least two generations of chlorite-like phyllosilicates, one prior to the main stage of deformation and the other coetaneous with the deformation.

XRD data

The oriented XRD powder patterns obtained from the air-dried and ethylene glycol-solvated samples are very similar, showing intense basal reflections typical of Mg-rich chlorite (Figure 4a,b), although glycolation caused a notable decrease and a slight broadening of the first basal reflection. In addition, the patterns show broad and very weak bands between the more intense reflections. Heating of samples caused splitting of the basal reflections, revealing the presence of two different phases: chlorite and a phase that contracted somewhat after heating. The latter phase is interpreted as mixed-layer chlorite-vermiculite in which the vermiculitic component contracted from 14 Å to 10 Å after heating (Figure 4c). Mixed layers showed broader reflections than chlorite in the pattern obtained after heating. Simulation of the chlorite pattern using *WinStruct* (Krumm, 1999), and using the chemical data shown below, suggested a sudoite composition (Figure 5a), whereas simulation of the mixed-layered structure using *NEWMOD* (Reynolds, 1985) was inconclusive because the intensity of the reflection of the mixed-layer structure, which overlaps with those of chlorite in the patterns of the untreated and glycolated samples, is unknown. Based on the position, intensity, and shape of the odd reflections, the simulated patterns suggest the presence of dominant chlorite (0.67):vermiculite (0.33) sequences with R = 1 (Figure 5b). Two main reflections were observed in the patterns obtained from unoriented samples in the zone of the 060 reflections (not shown): an intense reflection at 1.548 Å, corresponding to a trioctahedral phase and a second, less intense reflection at 1.509 Å, which indicated the presence of a di,trioctahedral one. In addition, a weak reflection at 1.499 Å suggested the presence of minor kaolinite.

SEM data

The SEM images show that variations in color and birefringence are mainly due to the variable degree of

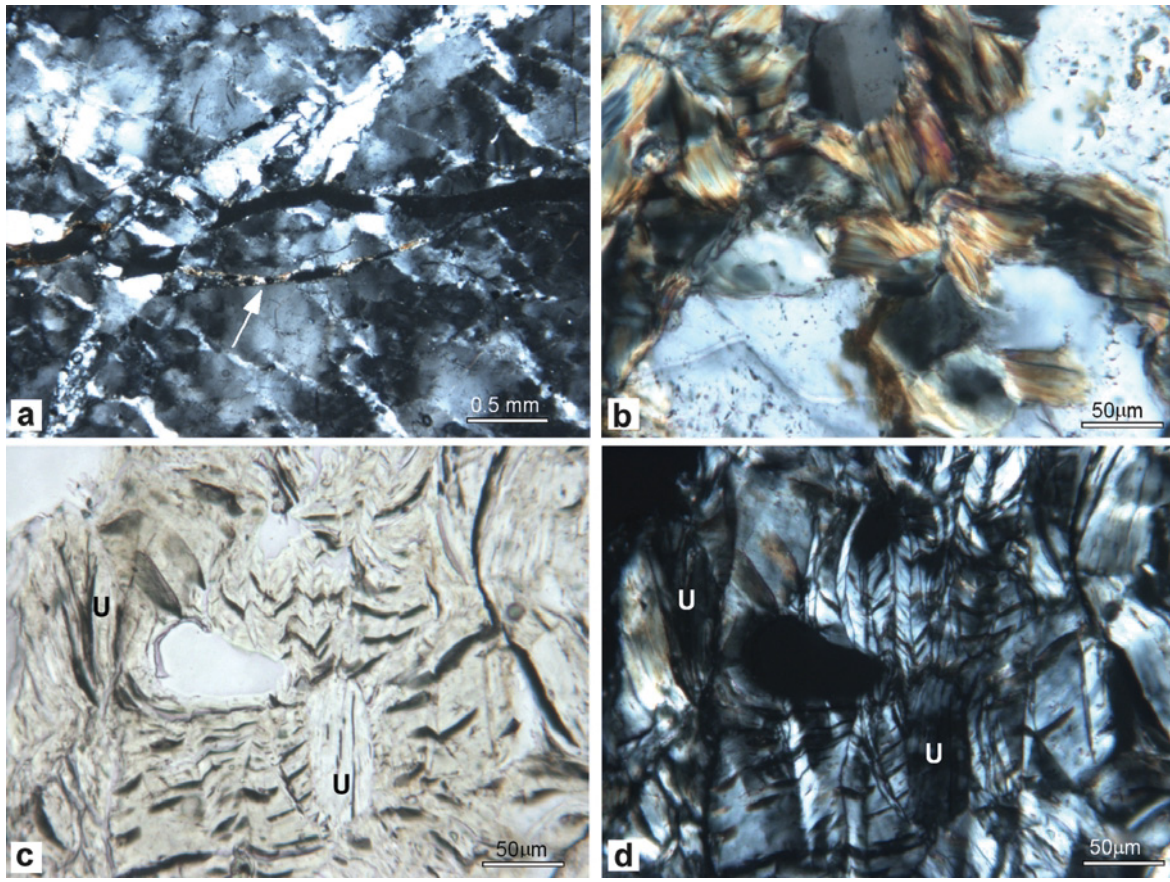

Figure 3. Petrographic microscopic images showing the deformation features in minerals from veins. (a) Quartz shows marked undulatory extinction and abundant recrystallization. Arrows indicate a thin veinlet filled by chlorite-like minerals. (b) Brown chlorite-like grains with variable interference color (crossed nicols). (c,d) Areas with strongly deformed chlorite-like grains (parallel and crossed nicols). Deformed grains vary in color from colorless to light green and show low birefringence. Undeformed grains (U) with orientation perpendicular to the compressive stress can also be observed.

retrogression of some chlorite grains to Fe oxide (Figure 6a). This appears to be a late alteration which mainly affected the external parts of some grains. In contrast, unaltered but variably deformed grains showed similar contrast, suggesting scarce compositional differences (Figure 6b–d). Deformation features are better observed at the SEM scale, in the back-scattered images, and include kinks (Figure 6a), chevron-like folds (Figure 6c), and fractures (Figure 6d). Some other smaller grains, defining an incipient schistosity or sealing fractures, appear clearly undeformed (Figure 6b). The EDX spectra revealed that variably deformed grains have Mg-rich compositions, the main variations affecting the Si and Al contents. Although the presence of minor amounts of Na and Ca suggests that most analyzed grains are not true chlorite, all formulae have been calculated for $O_{10}(OH)_8$ to aid comparison. Some representative formulae are reported in Table 1, with some illustrative chemical plots given in Figure 7. The Al *vs.* Si plot clearly reveals two populations of analyses with different Al contents (Figure 7a); the Al-richer population includes both deformed and undeformed grains. Some of these Al-rich analyses may correspond (see below) to grains containing kaolinite, as indicated by their deviation toward the kaolinite field. After elimination of these analyses, the plots from deformed grains show well defined trends in the ^{VI}Al *vs.* Si, Fe+Mg *vs.* Si, and octahedral occupancy *vs.* Si plots (Figure 7b–d). The trends could represent typical chlorite substitutions or simply mixtures of several phases in variable amounts. When the fields of clinochlore and sudoite are included in these plots, the analyses vary between the Mg-rich clinochlore term with Si = 2.8 atoms per formula unit (a.p.f.u.) and a more aluminous term near the composition of Fe-rich sudoite (Ruiz Cruz and Sanz de Galdeano, 2005). Deviations from the clinochlore and sudoite compositions strongly suggest the variable contribution of a Si- and (Fe+Mg)-richer phase, interpreted as corresponding to the vermiculite layers interstratified with chlorite. On the whole, the chemical data obtained at the SEM scale suggest lack of analyses of pure phases but rather

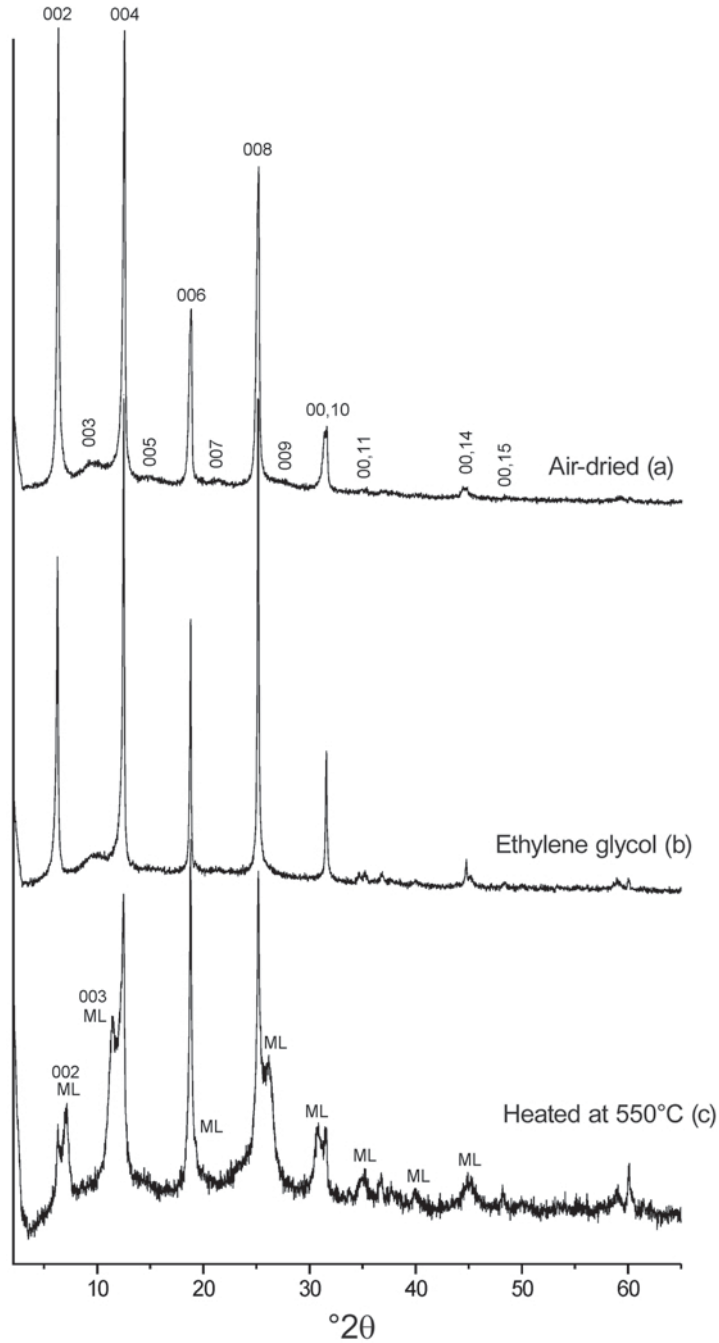

Figure 4. XRD patterns (2–65º2θ CuKα) obtained from oriented samples (a) after air-drying, (b) after ethylene-glycol solvation, and (c) after heating at 550ºC. The reflections ascribed to the mixed-layer (ML) phase have been labeled, assuming a regular 1:1 chlorite:vermiculite sequence.

mixtures of di,tri- and trioctahedral phases. Nevertheless, some deformed grains (*e.g.* analyses 7, 8, and 10, Table 1) show compositions near Tschermak-substituted Fe-rich sudoite, which probably contains large amounts of Fe(III) (Ruiz Cruz and Sanz de Galdeano, 2005), with octahedral occupancies on the order of 5.20 a.p.f.u. and ^{VI}Al contents of ~2.0 a.p.f.u..

TEM study

In contrast with bedding- or schistosity-parallel phyllosilicates, which are characteristic of the sedimentary and metamorphic rocks, chlorite grains included in the quartz veins described here are randomly oriented. The angle between the direction of metamorphic stress and the (001) planes of chlorite, which appears to be an

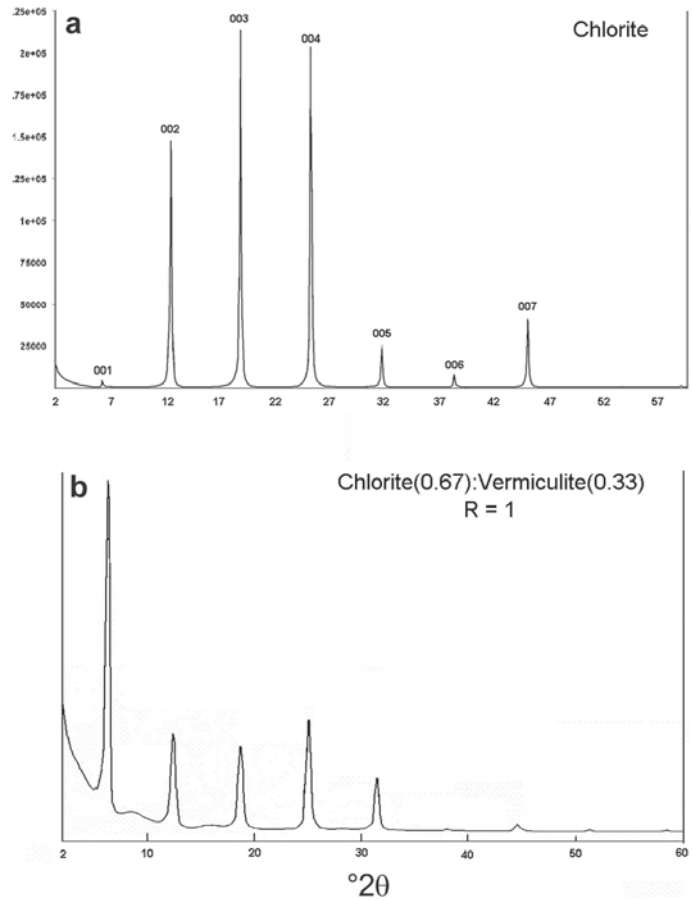

Figure 5. Simulated XRD patterns of chlorite (a) and mixed-layer chlorite-vermiculite (b).

important factor influencing the type of deformation (Etheridge *et al.*, 1973; Schneider, 1978), is therefore variable from grain to grain. Several states of deformation were attained in the different grains.

Table 1. Chemical data for deformed and undeformed chlorite-like grains, obtained at the SEM scale (formulae calculated for $O_{10}(OH)_8$).

	1 (a)	2 (a)	3 (b)	4 (b)	5 (b)	6 (b)	7 (c)	8 (c)	9 (c)	10 (c)	11 (c)	12 (c)	13 (c)	14 (d)	15 (d)
Si	3.24	3.10	3.01	3.10	2.90	3.10	3.45	3.38	3.23	3.43	3.19	3.15	3.33	3.17	3.49
^{IV}Al	0.76	0.90	0.99	0.90	1.10	0.90	0.55	0.62	0.77	0.57	0.81	0.85	0.67	0.83	0.51
^{VI}Al	1.46	1.43	1.39	1.40	1.33	1.38	2.02	2.01	1.65	1.89	1.64	1.40	1.59	1.46	1.79
Ti	0.00	0.00	0.00	0.01	0.00	0.00	0.00	0.00	0.01	0.00	0.00	0.00	0.00	0.00	0.00
Cr	0.01	0.00	0.00	0.00	0.00	0.00	0.00	0.00	0.00	0.00	0.00	0.00	0.01	0.00	0.00
Fe	1.18	1.22	1.24	1.26	1.38	1.29	0.98	0.98	1.16	1.05	1.17	1.21	1.18	1.27	1.21
Mn	0.01	0.01	0.01	0.01	0.02	0.01	0.00	0.01	0.01	0.01	0.01	0.01	0.01	0.02	0.01
Mg	2.92	3.03	3.10	3.02	3.15	3.01	2.17	2.20	2.60	2.26	2.68	3.00	2.62	2.86	2.19
ΣOct	5.57	5.68	5.75	5.70	5.88	5.70	5.16	5.21	5.43	5.22	5.50	5.61	5.41	5.61	5.19
Ca	0.04	0.03	0.03	0.03	0.01	0.04	0.05	0.04	0.03	0.04	0.03	0.04	0.05	0.04	0.08
Na	0.03	0.04	0.04	0.00	0.00	0.02	0.06	0.04	0.07	0.08	0.06	0.08	0.05	0.05	0.10
K	0.02	0.01	0.01	0.02	0.00	0.02	0.05	0.07	0.09	0.08	0.06	0.08	0.05	0.03	0.09
ΣInt	0.09	0.08	0.07	0.05	0.01	0.08	0.16	0.15	0.19	0.20	0.15	0.19	0.16	0.12	0.26

(a), (b), (c), and (d) refer to the relevant part of Fig. 6.

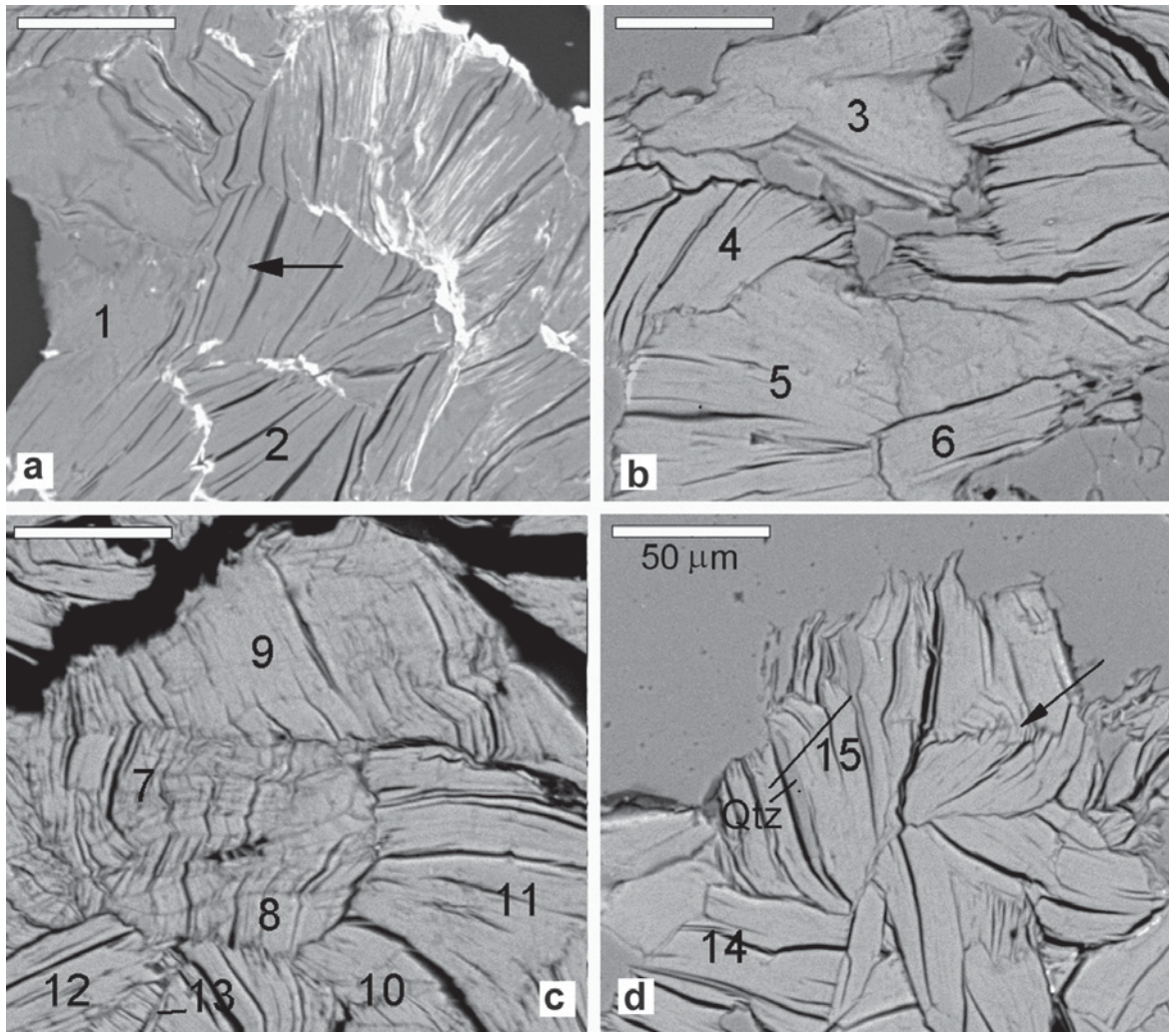

Figure 6. Back-scattered images of the several chlorite-like minerals. (a) Grains with an advanced degree of alteration to Fe oxide. The arrow indicates a kink. (b) Slightly deformed grains. (c) Area with chevron-like folds and undeformed grains (lower left corner). (d) Fractured grains (arrow) and thin intergrowths of 'chlorite'-quartz. The numbers correspond to analyses in Table 1. The scale-bar is common to all the images.

In most cases, deformed grains could be easily identified at low magnification because they showed textural features similar to those observed at the SEM scale. The presence in phyllosilicates of only one slip plane (001) is responsible for their characteristic modes of deformation, which mainly involve basal slips, basal cleavages, bending, and kinking mechanisms (Amouric, 1987).

Incipient deformation is reflected in some areas on folds with large radius of curvature (Figure 8a). Incipient deformation causes a series of microcleavages produced by basal slip, similar to those shown by Amouric (1987) in metamorphic biotite (Figure 8a), although the grains maintain a dominant 14 Å chlorite structure (Figure 8b). Stacking faults, wavy layers, and edge dislocations are also common. The selected area electron diffraction (SAED) patterns obtained from these grains (Figure 8b, inset) showed basal reflections with intensity distribution typical of sudoite (Bailey and Lister, 1989; Anceau, 1992).

Chevron-type folds, identified in the petrographic and back-scattered images (Figures 3c,d, 6c), and showing wavelengths of 20–50 μm, are interpreted as revealing a greater degree of deformation and are characterized by polygonal-shaped microcleavages, aligned along the axial planes of the folds (Figure 9a,b), similar to those described previously (*e.g.* Amouric, 1987; Sánchez-Navas and Galindo-Zaldívar, 1993). At the scale of the TEM these areas provided SAED patterns revealing almost symmetrical orientation of both sides of the fold. Nevertheless, the hinges are strongly damaged and the structural relations between adjacent sectors cannot be

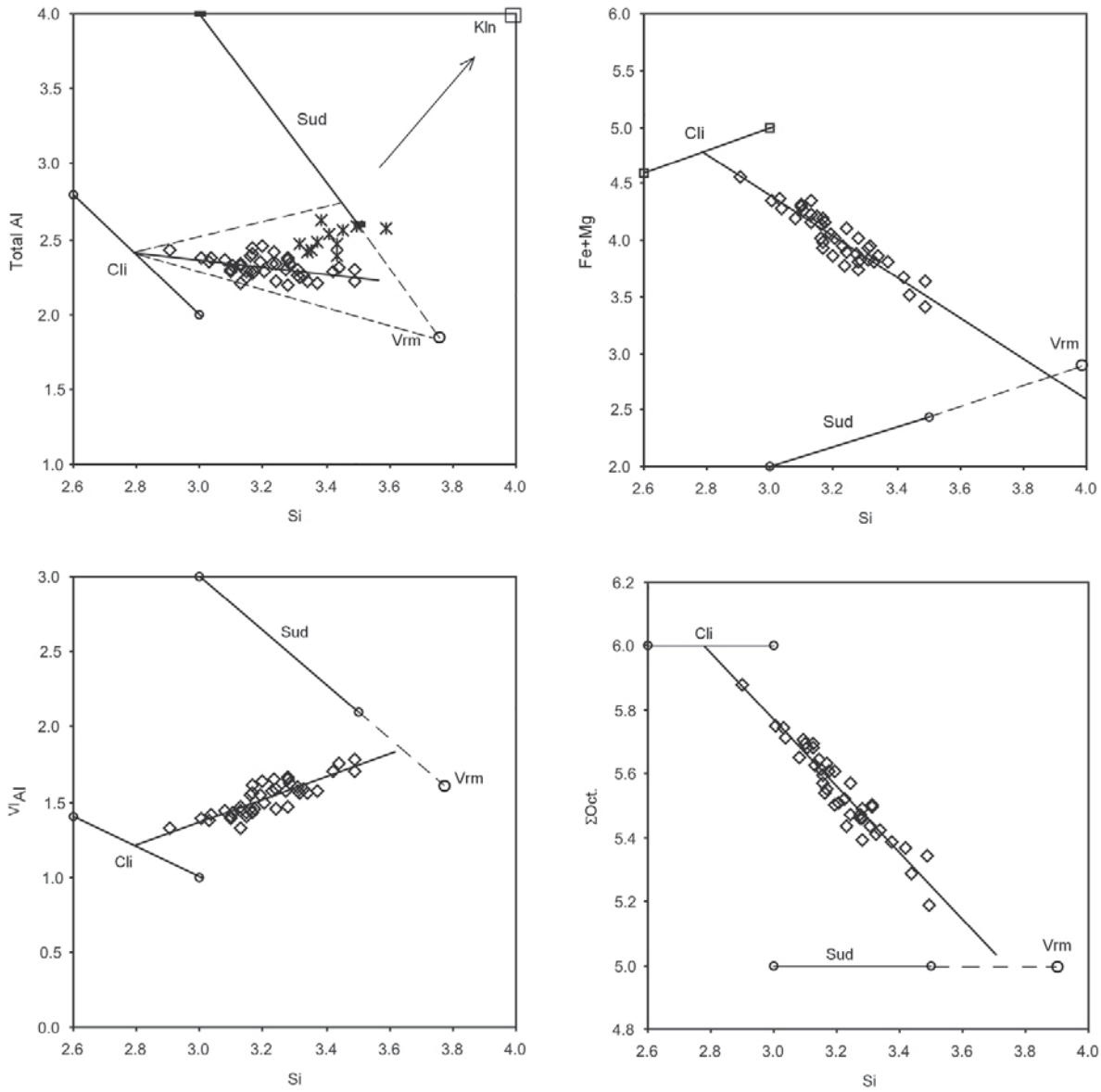

Figure 7. Chemical plots showing the compositional variation of chlorite-like minerals at the SEM scale. ×: deformed and undeformed Al-rich grains; ◇: deformed grains. The fields of clinochlore (Cli) and Tschermak- and Fe-substituted sudoite have been included for comparison. All of the analyses require the contribution of a Si-rich and Fe+Mg-richer phase, which must correspond to the vermiculitic component (Vrm) of the mixed-layer structure.

observed directly. Lattice-fringe images and SAED patterns revealed that most grains consist of thick packets, which include chlorite and mixed-layer chlorite-vermiculite areas (Figure 10a). Chlorite and mixed-layer chlorite-vermiculite appear as discontinuous domains on the order of a few hundred Å thick, with boundaries parallel and oblique to the basal planes. The SAED patterns (Figure 10a, inset) showed parallelism of c^* and b^* in mixed-layer chlorite-vermiculite and chlorite, and almost continuous 0*kl* reflection rows, probably due to overlapping of the chlorite and mixed-layer reflections, in addition to possible stacking disorder. Although mixed-layer sequences regularly showed a periodicity of ~24 Å, corresponding to 1 chlorite (14 Å) + 1 contracted vermiculite (10 Å) layers (corrensite), sequences with a 38 Å periodicity (2 chlorite + 1 contracted vermiculite layers) are also common (Figure 10b).

The SEM images showed that chlorite grains are fractured locally (Figure 6d). Generally, the fractured grains are very unstable under the electron beam (*i.e.* the external thinned areas are detached during examination), and good images of these grains are difficult to obtain. Figure 11 shows an example of this type of grain. A later, undeformed grain grew, sealing the fracture. Late,

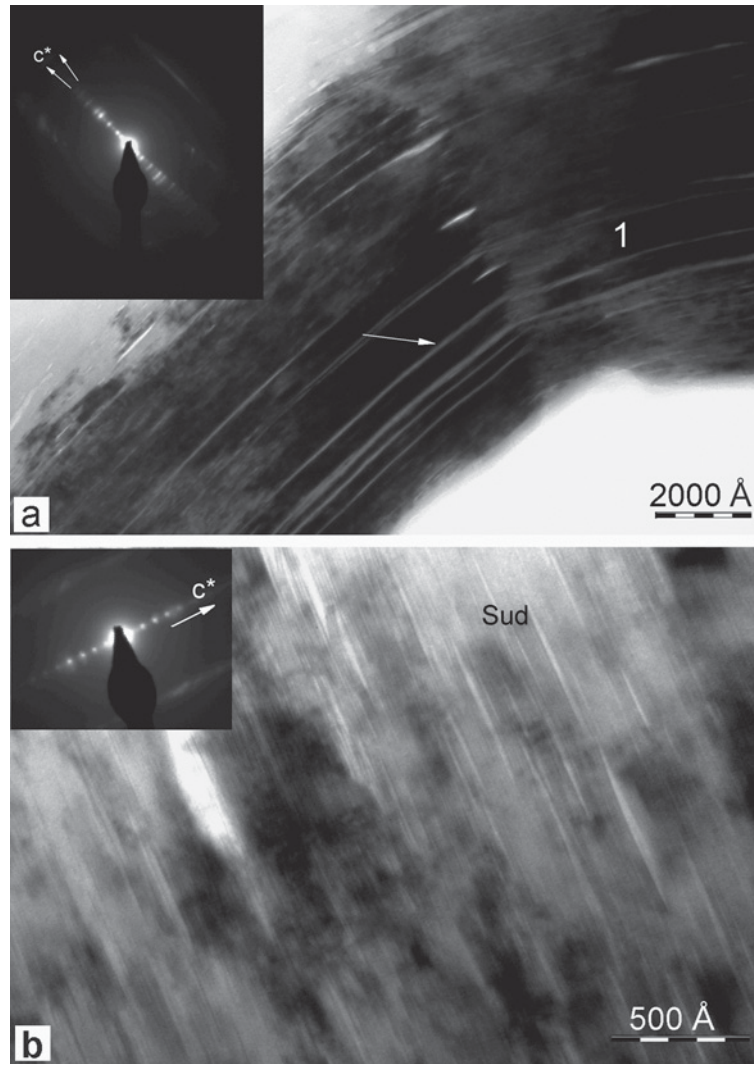

Figure 8. (a) Low-magnification TEM image of a folded grain. This consists of sub-parallel packets with variable curvature radius. The deformation is revealed by the presence of numerous thin, parallel gray areas, which probably represent the contribution of vermiculite-like layers contracting against the electron beam and microcleavages (white arrow). (b) Lattice-fringe image of the less deformed area, showing the presence of lenticular voids probably caused by variable contraction of vermiculite layers. The SAED pattern (inset) shows the intensity distribution typical of sudoite.

undeformed grains consist, according to the information provided by the AEM data and SAED patterns of intergrowths, of several phases, mainly chlorite-vermiculite mixed-layers, kaolinite, and minor Fe oxide (Figure 12). In contrast to chlorite and chlorite-vermiculite intergrowths observed in the deformed grains, the intergrowths in the undeformed grains show coherent boundaries parallel to (001). Indeed, the SAED patterns indicate that both mixed-layer chlorite-vermiculite and kaolinite show parallelism of *c**, suggesting that kaolinite formed from retrogression of mixed-layer chlorite-vermiculite. Minute Fe-oxide grains are also present, showing elongation parallel to (001) of the host phyllosilicate.

AEM data

Because of the small size of the domains of several phases in both deformed and undeformed grains, the analyses obtained again corresponded to mixtures. As before, the formulae were calculated for $O_{10}(OH)_8$ to aid comparison (Table 2). The AEM data of late, undeformed grains generally showed the contribution of kaolinite, leading to a clear deviation toward Al-richer compositions, as also observed at the SEM scale (Table 2, analyses 5 and 6, Figure 13a). The analyses obtained from deformed, kaolinite-free grains, as deduced from the lattice-fringe images, showed some compositional variations, and two groups of analyses with different Si, ^{VI}Al, and (Fe+Mg) contents were

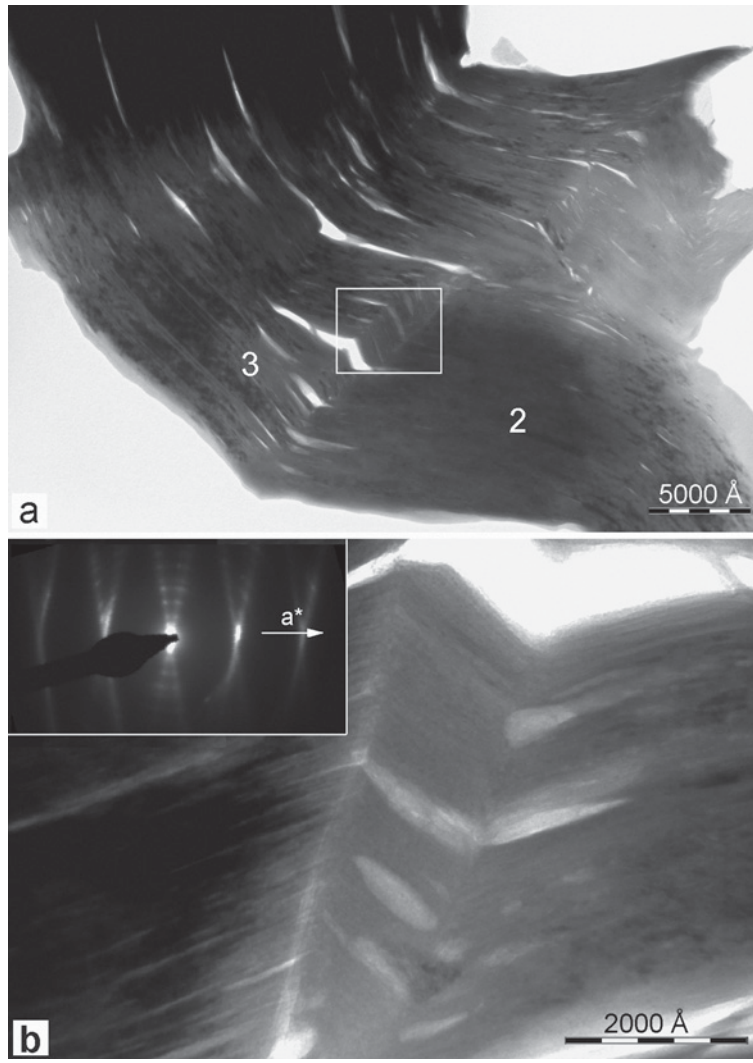

Figure 9. (a) Strongly deformed grain, showing polygonal microcleavages aligned along the axial planes of the folds. (b) Close-up of part a. The SAED pattern (inset) shows the almost symmetrical orientation of both sides of the fold. The numbers correspond to analyses in Table 2.

Table 2. Selected AEM data for grains shown in Figures 8, 9, 11, and 12.

	1 Figure 8	2 Figure 9	3 Figure 9	4 Figure 11	5 Figure 11	6 Figure 11	7 Figure 12	8 Figure 12	9 Figure 12
Si	3.33	3.35	3.03	3.35	3.39	3.45	3.14	3.07	2.97
^{IV}Al	0.67	0.65	0.97	0.65	0.61	0.55	0.86	0.93	1.03
^{VI}Al	1.95	1.68	1.75	1.66	2.32	2.39	1.74	1.43	1.35
Fe	1.05	1.04	1.35	1.06	0.86	0.86	1.11	1.05	1.17
Mn	0.00	0.00	0.02	0.02	0.00	0.00	0.00	0.02	0.00
Mg	2.25	2.62	2.39	2.71	1.86	1.78	2.64	3.14	3.12
ΣOct	5.25	5.33	5.51	5.45	5.03	5.02	5.49	5.64	5.64
Ca	0.05	0.07	0.02	0.02	0.05	0.02	0.02	0.02	0.10
Na	0.12	0.16	0.12	0.09	0.16	0.09	0.12	0.10	0.26
K	0.00	0.00	0.00	0.02	0.00	0.00	0.00	0.02	0.00
ΣInt	0.16	0.24	0.14	0.14	0.21	0.12	0.14	0.14	0.36

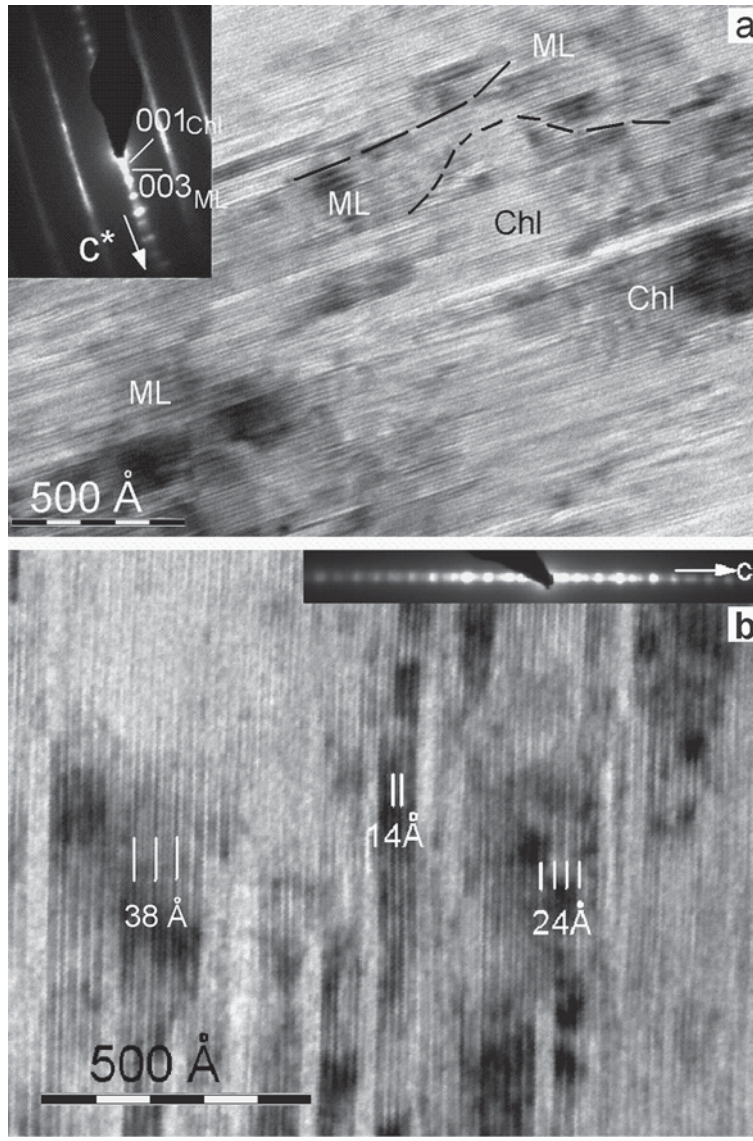

Figure 10. (a) Domainal texture in deformed grains. Variably sized chlorite (Chl) and mixed-layer (ML) domains appear to be irregularly distributed and show both parallel and oblique boundaries. The SAED pattern (inset) shows reflections of both types of phases. (b) HRTEM imaging of parallel intergrowths of chlorite (14 Å) and several types of chlorite-vermiculite mixed-layers, with dominant 24 and 38 Å periodicities.

differentiated (Figure 13). Some slightly deformed grains (*e.g.* Figure 8, Table 2, analysis 1) showed ^{VI}Al contents of $\geqslant$2.0 a.p.f.u. and octahedral occupancies near 5.0 a.p.f.u., the average formula being near that of Fe-rich sudoite. The other group had smaller Si contents and larger octahedral occupancies, indicating a deviation toward trioctahedral terms. Nevertheless, even sudoite analyses contain significant amounts of Na, which is difficult to explain because the lattice-fringe images of these grains indicated an almost uniform chlorite periodicity (Figure 8b). Curiously, some analyses of late grains consisting of intergrowths of mixed-layer chlorite-vermiculite and kaolinite also provided analyses with low octahedral occupancies and Al-rich compositions (Table 2, analyses 5 and 6), and they could be easily mistaken for sudoite at the SEM scale.

DISCUSSION

In the following discussion, sudoite-bearing quartz veins are interpreted as having formed through a process of metamorphic segregation during prograde evolution, as previously interpreted by Bouybaouène (1993). Indeed, veins and enclosing phyllites share the same deformation features. Nevertheless, in contrast with most observations in metamorphic terranes, as well as

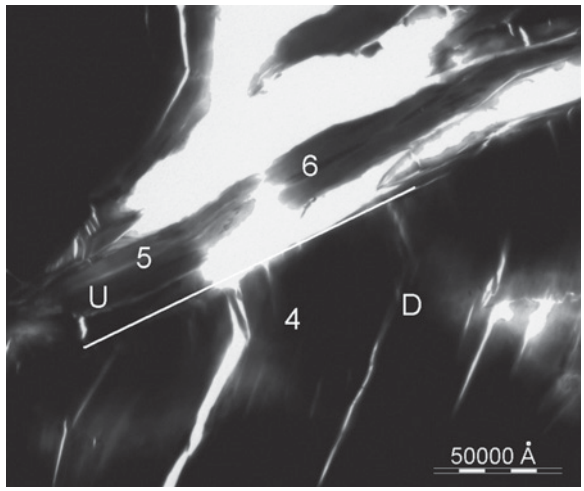

Figure 11. Low-magnification image of a deformed and fractured grain (D). A later, undeformed grain (U) grew, sealing the fracture. The numbers correspond to analyses in Table 2.

in veins from Triassic formations of the Betic-Rif range where the minerals found in the veins are generally present in the enclosing rocks, in this case the mineral assemblages in phyllites and veins are rather different. For example, sudoite has not been found in the enclosing phyllites, whereas white mica and talc have not been found in veins. Veins are relatively enriched in Mg and Fe. In contrast, most Al, K, Na, and Ca remained in the enclosing white mica-rich phyllites, probably as an effect of the metamorphic reactions occurring later.

Deformation features and compositional changes

Incipient deformation is obvious in the TEM images (Figure 8). Adjustment between successive layers or packets of layers could have occurred during this early stage either through the presence of regularly distributed dislocations or through basal slips. Slip parallel to the basal planes produced variably sized microcleavages, which were probable paths for fluid circulation and incipient vermiculitization. Na found in analyses of these grains is probably lodged in defect-rich areas of these grains.

More advanced deformation is shown by the presence of kink and chevron-like folds. Accommodation of the compressive stress in these more deformed grains gave rise to polygonal microcleavages aligned along the axial planes of the folds (Figure 9), as previously observed by other authors (Bell and Wilson, 1981; Amouric, 1987; Sánchez-Navas and Galindo-Zaldívar, 1993). Moreover, intense deformation is accompanied by structural changes consisting of a more generalized and ordered vermiculitization process, leading to domains of chlorite and of mixed-layer chlorite-vermiculite. Because the electrostatic bonding between brucite sheets and talc layers is stronger than between vermiculite layers, gliding and accommodation of the compressive stress is favored by the replacement of brucite sheets by hydrated sheets.

These structural changes led to the associated chemical changes. Although analyses of pure phases have not been obtained, the trends observed (Figures 7, 13) suggest that vermiculitization of sudoite mainly implied enrichment in Fe+Mg. The 'porosity' due to the presence of larger microcleavages probably favored the mass transfer through the deformed grains. Lattice-fringe images (Figure 14) show abundant transitions between chlorite- and mixed-layer domains. Although the transitional areas are rapidly damaged under the beam, they appear to include: (1) transitions from two chlorite layers (28 Å) to one mixed-layer unit (24 Å), the most frequent (Figure 14a,b); and (2) transitions from

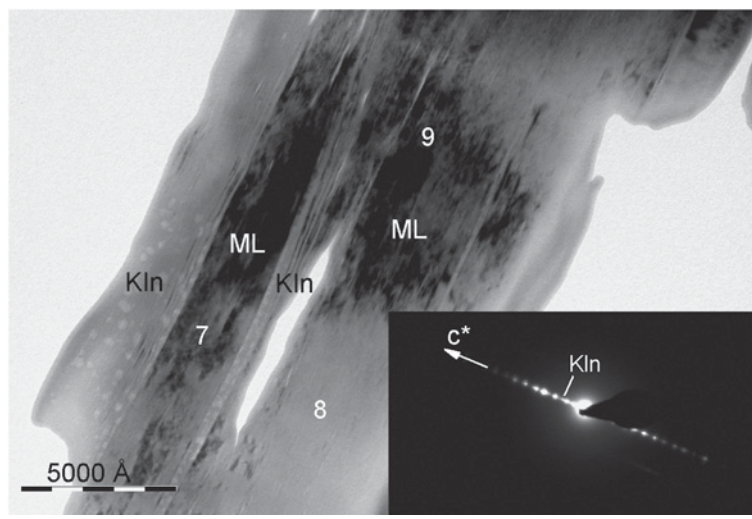

Figure 12. Low-magnification TEM image showing a parallel kaolinite (Kln)-mixed-layer (ML) intergrowth. The SAED pattern (inset) shows reflections of the two phases. The numbers correspond to analyses in Table 2.

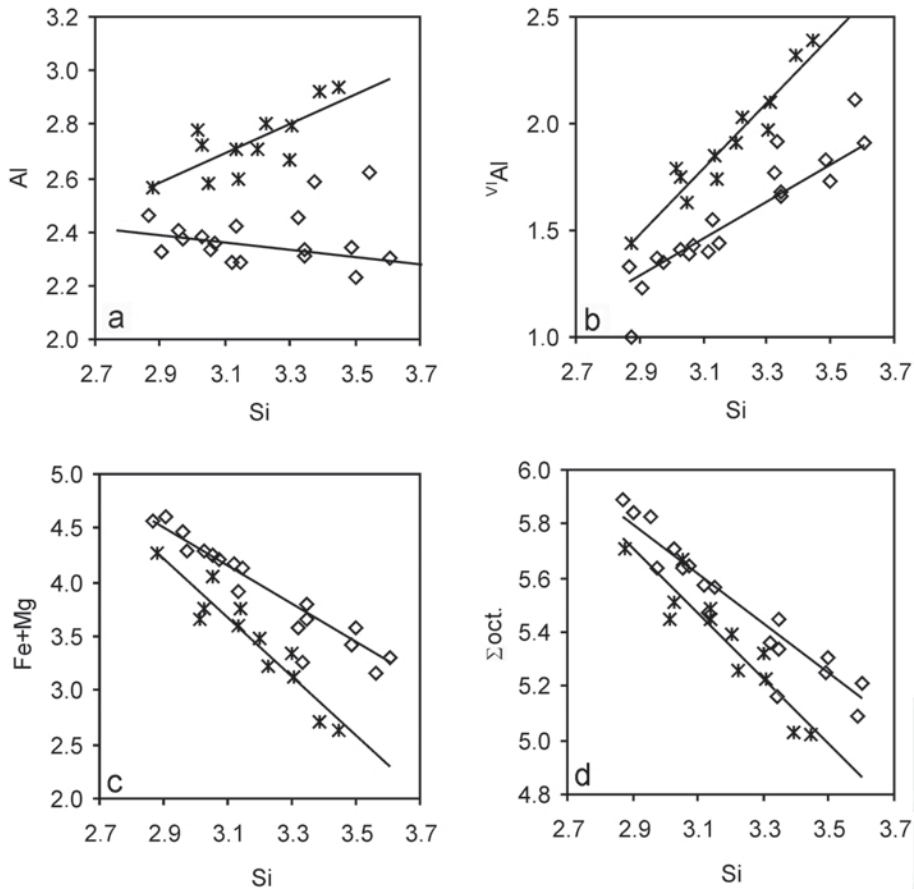

Figure 13. Chemical plots showing the compositional variations of undeformed (×) and deformed (◇) grains, at the TEM scale.

one chlorite layer (14 Å) to one mixed-layer unit (24 Å), associated with dislocations (Figure 14a,c). Dislocations of opposite sign are common, defining the oblique boundaries between chlorite and mixed-layer domains, suggesting that octahedral cations from the brucite sheets (Mg and Fe) were removed from every second or third interlayer of sudoite and incorporated into the talc sheets, leading to semi-regular 1:1 and 2:1 interstratifications of chlorite-vermiculite. Resulting intergrowths of chlorite and mixed layers retain the primary chlorite orientation and morphology, indicating a topotactic replacement. Although the shape of the domains with different structure is variable, the numerous transitions from chlorite- to mixed-layer domains suggest that diffusion was very limited in the space.

Microscopic images obtained at very different scales (*e.g.* Figures 3c, 11) showed that undeformed grains have basal planes perpendicular to the compressive stress, in some cases sealing the fractures affecting the deformed grains. Dissolution-precipitation may, therefore, have been responsible for this formation during deformation. Nevertheless, although this process must have occurred locally, it is not generalized. Most of these grains also show complex microstructures (Figure 12), consisting of parallel intergrowths of kaolinite, mixed-layer chlorite-vermiculite, and minor Fe oxide, suggesting low-temperature formation. The several phases showed in these grains continuous packets of layers and coherent boundaries parallel to (001), suggesting that these later grains consisted mainly of mixed layers and, in turn, were preferentially retrograded to kaolinite.

Tectono-metamorphic history

The formation of sudoite in units intermediate between typical Sebtide (Alpujárride) and Ghomaride (Maláguide) units has been described in some areas of the Betic-Rif range (Bouybaouène, 1993; Bouybaouène *et al*., 1995**;** Ruiz Cruz and Sanz de Galdeano, 2005). Nevertheless, whereas in the Boquete de Anyera unit of the Rif, sudoite has been interpreted as forming from the reaction of clinochlore and pyrophyllite (Bouybaouène, 1993; Bouybaouène *et al*., 1995; Michard *et al*., 1997), sudoite found in Maláguide- and Alpujárride-like intermediate units from the Betic zone (Ruiz Cruz and Sanz de Galdeano, 2005) mainly formed from dickite. Sudoite described from the latter area includes typical Mg-rich terms and terms containing significant amounts of Fe(II)

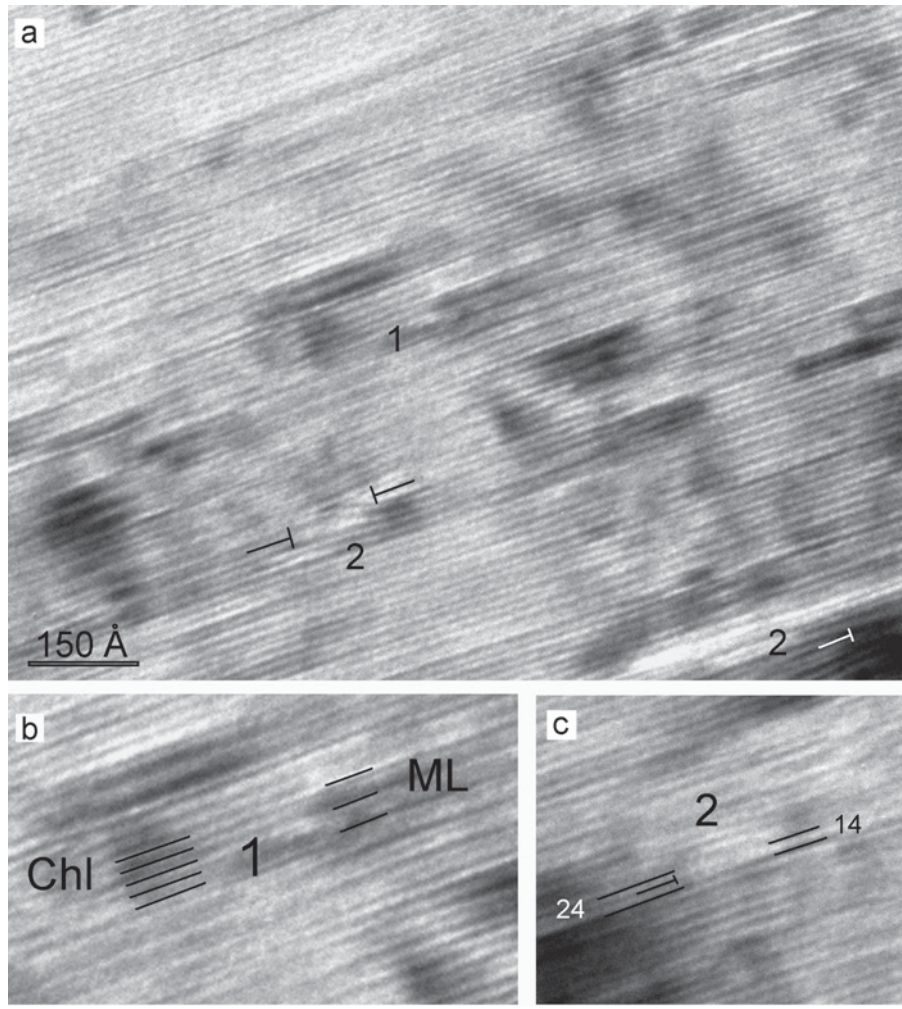

Figure 14. (a) Lattice-fringe image showing the main types of layer transitions. 1: Transition from two chlorite layers (28 Å) to one chlorite-vermiculite layer (24 Å). 2: Transitions from a chlorite (14 Å) to one chlorite-vermiculite layer (24 Å), associated with the gain of a vermiculite layer. (b,c) Enlarged views of the transition zones.

and Fe(III). The data presented here indicate that sudoite from veins described here is probably near the Fe-rich term. The possibility that sudoite formed as a breakdown product of carpholite (Vidal *et al*., 1992) can be discarded taking into account that carpholite relics have not been identified at this zone and that the quartz/sudoite ratio in veins is notably greater than that expected from carpholite breakdown. Lack of pyrophyllite and kaolin-type minerals in the enclosing phyllites suggests that quartz+chlorite-rich veins formed during illitization of smectite-rich sediments. The available data point to a deduction that sudoite formed in veins at temperatures of <350ºC and at pressure of <7 kbar (Vidal *et al.*, 1992).

Sudoite was deformed during a later compressive episode. Retrogression of chlorite to corrensite and other types of chlorite-smectite or mixed-layer chlorite-vermiculite from weathering processes has been described by numerous authors (*e.g.* Aspandiar and Eggleton, 2002a, 2000b; Sugimori *et al*., 2008) and a detailed study of the structural changes occurring during weathering was carried out by Banfield and Murakami (1998). Although retrogression of chlorite (dissolution and Fe-oxide formation) occurred well after the deformation of the samples described here, vermiculitization seems to be clearly coetaneous with deformation, as confirmed by the persistence of unaltered sudoite in the less deformed grains as well as by textures in the enclosing phyllites, which demonstrate that vermiculite grew during the compressive stage (Figure 2). Parallelism of c^* and b^* of the products with the host chlorite (*e.g.* Figure 10a) indicates topotactic alteration.

The maximum temperatures attained in this area during the later exhumation process have been estimated as <330ºC (Negro *et al*., 2006). Indeed, because the assumed reaction (chlorite vermiculitization) implies some hydration, one can assume that retrogression of

sudoite occurred during the last stage of exhumation and cooling. Exhumation has been dated at 22–18 Ma (Zeck, 2004). Given the structural position of these units in the Gibraltar arc, the latest plastic deformations probably occurred during translations toward the west during the lower Miocene.

CONCLUSIONS

Sudoite-bearing quartz-rich veins enclosed in phyllites from the lowest Federico unit (Internal Zone of the Rif belt) were modified extensively during deformation and retrogression. Deformation includes kinks, chevron-like folds, and minor fractures in chlorite grains and plastic deformation and recrystallization in quartz. Deformation of chlorite grains was accompanied by chemical and structural modifications that produced regular (high-charge corrensite) and randomly ordered mixed-layer chlorite-vermiculite. From the data presented, the ordered replacement of a brucite sheet by a hydrated one is clearly an effective mechanism for favoring slip and for accommodation of the compressive stress during deformation. Retrogression of sudoite probably occurred during the latest stage of exhumation under low-temperature conditions.

ACKNOWLEDGMENTS

The authors are grateful to T. Kogure, A. Baronnet, and two unknown reviewers whose suggestions and corrections notably improved the manuscript. Thanks to M.M. Abad (CIC, Universidad de Granada) for help in obtaining TEM/AEM data. This study received financial support from Project CGL 2006-02481 (Ministerio de Educación y Ciencia) and from the Research Group RNM-199 (Junta de Andalucía).

REFERENCES

Amouric, M. (1987) Growth and deformation defects in phyllosilicates as seen by HRTEM. *Acta Crystallographica*, **B43**, 57–63.

Anceau, A. (1992) Sudoite in some Visean (lower Carboniferous) K-bentonites from Belgium. *Clay Minerals*, **27**, 283–292.

Aspandiar, M.F. and Eggleton, R.A. (2002a) Weathering of chlorite. I. Reactions and products in microsystems controlled by the primary minerals. *Clays and Clay Minerals*, **50**, 685–698.

Aspandiar, M.F. and Eggleton, R.A. (2002b) Weathering of chlorite. II. Reactions and products in microsystems controlled by solution avenues. *Clays and Clay Minerals*, **50**, 699–709.

Azañón, J.M. and Goffé, B. (1997) Ferro- and magnesiocarpholite assemblages as a record of high-*P*, low-*T* metamorphism in the Central Alpujárrides, Betic Cordillera (SE Spain). *European Journal of Mineralogy*, **9**, 1035–1051.

Azañón, J.M., García-Dueñas, V., and Goffé, B. (1992) High pressure mineral assemblages in the Trevenque unit (Central Alpujárrides, Andalucía). *Geogaceta*, **11**, 81–84

Bailey, S.W. and Lister, J.S. (1989) Structures, compositions and X-ray identification of dioctahedral chlorites. *Clays and Clay Minerals*, **37**, 193–202.

Banfield, J.F. and Murakami, T. (1998) Atomic-resolution transmission electron microscope evidence for the mechanism by which chlorite weathers to 1:1 semi-regular chlorite-vermiculite. *American Mineralogist*, **83**, 348–357.

Baronnet, A. and Olives, J. (1983) The geometry of micas around kink band boundaries. I. Crystallographic model. *Tectonophysics*, **91**, 359–373.

Bell, I.A. and Wilson, C.J.L. (1981) Deformation of biotite and muscovite: TEM microstructure and deformation model. *Tectonophysics*, **78**, 201–228.

Bell, I.A. and Wilson, C.J.L. (1986) TEM observation of defects in biotite and their relationships to polytypism. *Bulletin de Minéralogie*, **109,** 163–170.

Bell, I.A., Wilson, C.J.L., McLaren, A.C., and Etheridge, M.A. (1986) Kinks in mica: role of dislocations and (001) cleavage. *Tectonophysics*, **127**, 49–65.

Bouybaouène, M.L. (1993) Étude pétrologique des metapélites Sebtides supérieures, Rif Interne, Maroc: Une évolution métamorphique de haute pression. PhD thesis, Université Mohammmed V. Rabat, Morocco, 151 pp.

Bouybaouène, M.L., Goffé, B., and Michard, A. (1995) High-pressure, low-temperature metamorphism in the Sebtide nappes, northern Rif, Morocco. *Geogaceta*, **17**, 117–119.

Cliff, G. and Lorimer, G.W. (1975) The quantitative analysis of thin specimens. *Journal of Microscopy*, **103**, 203–207.

Didon, J., Durand-Delga, M., and Kornprobst, J. (1973) Homologies géologiques entre les deux rives du Détroit de Gibraltar. *Bulletin de la Societée Géologique de France*, **15**, 77–105.

Etheridge, M.A., Hobbs, B.E., and Paterson, M.S. (1973) Experimental deformation of single crystals of biotite. *Contributions to Mineralogy and Petrology*, **38**, 21–36.

Goffé, B., Michard, A., García-Dueñas, V., González-Lodeiro, F., Monié, P., Campos, J., Galindo-Zaldívar, J., Jabaloy, A., Martínez-Martínez, J.M., and Simancas, J.F. (1989) First evidence of high-pressure, low-temperature metamorphism in the Alpujárride nappes, Betic Cordillera (SE Spain). *European Journal of Mineralogy*, **1**, 139–142.

Jiménez-Millán, J., Vázquez, M., and Velilla, N. (2007) Deformation-promoted defects and retrograde chloritization of biotite in slates from a shear zone, southern Iberian massif, SE Spain. *Clays and Clay Minerals*, **55**, 285–295.

Knipe, R.J. (1981) The interaction of deformation and metamorphism in slates. *Tectonophysics*, **78**, 249–272.

Kornprosbt, J. (1971–1974) Contribution à l'étude pétrographique et structurale de la zone interne du Rif (Maroc septentrional). *Notes Mémoires Service Géologique Maroc*, **251**, 256 pp.

Kretz, R. (1994) *Metamorphic Crystallization*. John Wiley & Sons, Chichester, UK & New York.

Krumm, S. (1999) Simulation of XRD patterns from oriented clay minerals with WinStruct. *Computers & Geoscience*, **25**, 501–509.

Michard, A., Goffé, B., Bouybaouène, M.L., and Saddiqi, O. (1997) Late Hercynian-Mesozoic thinning in the Alboran domain: metamorphic data from the northern Rif, Morocco. *Terra Nova*, **9**,171–174.

Negro, F., Beyssac, O., Goffé, B., Saddiqi, O., and Bouybaouène, L. (2006) Thermal structure of the Alboran domain in the Rif (northern Morocco) and the western Betics (southern Spain). Constraints from Raman spectroscopy of carbonaceous material. *Journal of Metamorphic Geology*, **24**, 309–327.

Olives, J., Amouric, M., Fouquet, C.D., and Baronnet, A. (1983) Interlayering and interlayer slip in biotite as seen by HRTEM. *American Mineralogist*, **68**, 754–758.

Ooteman, A., Ferrow, E.A., and Lindh, A. (2003) An electron microscopy study of deformation microstructures in granitic mylonites from southwestern Sweden, with special emphasis on the micas. *Mineralogy and Petrology*, **78**, 255–268.

Reynolds, R.C. (1985) *NEWMOD – A computer program for calculation of one-dimensional X-ray diffraction patterns of mixed-layered clays*. 8 Brook Rd., Hanover, NH, USA.

Ruiz Cruz, M.D. and Sanz de Galdeano, C. (2005) Compositional and structural variation of sudoite from the Betic Cordillera (Spain): A TEM/AEM study. *Clays and Clay Minerals*, **53**, 639–652.

Ruiz Cruz, M.D., Sanz de Galdeano, C., Alvarez-Valero, A., Rodríguez Ruiz, M.D., and Novak, J. (2010) Pumpellyite and coexisting minerals in metapelites and veins from the Federico units in the Internal Zone of the Rif, Spain. *The Canadian Mineralogist*, **48**, 155–175.

Sánchez-Navas, A. and Galindo-Zaldívar, J. (1993) Alteration and deformation microstructures of biotite from plagioclase-rich dykes (Ronda Massif, S. Spain). *European Journal of Mineralogy*, **5**, 245–256.

Sanz de Galdeano, C., Andreo, B., García-Tortosa, F.J., and López-Garrido, A.C. (2001) The Triassic palaeogeographic transition between the Alpujárride and Maláguide complexes. Betic-Rif Internal Zone (S. Spain, N. Morocco). *Palaeogeography, Palaeoclimatology, Palaeoecology*, **167**, 157–173.

Schneider, H. (1978) Investigations on the deformation of experimentally stock-loaded biotites using X-ray single crystal diffraction techniques. *Mineralogical Magazine*, **42**, 41–44.

Sugimori, H., Iwatsuki, T., and Murakami, T. (2008) Chlorite and biotite weathering, Fe^{2+}-rich corrensite formation, and Fe behaviour under low P_{O_2} conditions and their implication for Precambrian weathering. *American Mineralogist*, **93**, 1080–1089.

Vernon, R.H. (1977) Microfabric of mica aggregates in partly recrystallized biotite. *Contributions to Mineralogy and Petrology*, **61**,176–185.

Vidal, O., Goffé, B., and Theye, T. (1992) Experimental investigation of the stability of sudoite and magnesiocarpholite and calculation of a petrogenetic grid for the system FeO-MgO-Al_2O_3-SiO_2-H_2O. *Journal of Metamorphic Geology*, **10**, 603–614.

Zeck, H.P. (2004) Rapid exhumation in the alpine belt of the Betic-Rif (W Mediterranean): Tectonic extrusion. *Pure and Applied Geophysics*, **161**, 477–487.

(*Received 23 January 2009; revised 5 August 2009; Ms. 227; A.E. T. Kogure*)